Sliding Mode Control Based Energy Harvesting System For Low Power Applications

Honorio Martinez Sarmiento Department of Electrical and Computer Engineering California State University, Fresno California, USA hsarmiento@mail.fresnostate.edu

Maen Marji Department of Electrical and Computer Engineering California State University, Fresno California, USA maen.marji@yahoo.com

Nan Wang Department of Electrical and Computer Engineering California State University, Fresno California, USA nwang@mail.fresnostate.edu

Cheaheng Lim Department of Electrical and Computer Engineering California State University, Fresno California, USA cheal@mail.fresnostate.edu

Jonghoon Kim Department of Electrical Engineering Chungnam National University, Daejon South Korea whdgns0422@cnu.ac.kr

Woonki Na Department of Electrical and Computer Engineering California State University, Fresno California, USA wkna@csufresno.edu

Abstract-As technology advances and cities become more innovative, the need to harvest energy to power intelligent devices at remote locations, such as wireless sensors, is increasing. This paper focuses on studying and simulating an energy management system (EMS) for energy harvesting with a battery and a supercapacitor for low power applications. Lithium-ion batteries are the primary energy storage source for low power applications due to their high energy density and efficiency. On the other hand, the supercapacitors excel in fast charge and discharge. Furthermore, supercapacitors tolerate high currents due to their low equivalent series resistance (ESR). The supercapacitor in the system increases the time response of the power delivery to the load, and it also absorbs the high currents in the system. Moreover, the supercapacitor covers short-time load demand due to the fluctuation of the renewable source. The EMS monitors the proposed system to maintain power to the load either from the renewable source or the energy storage. The power flow of the energy storage is controlled via DC-DC bidirectional converters. The lithium-ion battery is charged via a constant current (CC) using a sliding mode controller (SMC) and a constant voltage (CV) via a typical PI controller. The response of the SMC current controller is compared with PI and Fuzzy current controller. Furthermore, the performance of a system having and not having a supercapacitor is compared. Finally, MATLAB modeling system simulation and experimental implementation results are analyzed and presented.

Keywords— Energy Management System, Energy Harvesting, Lithium-ion Battery, Supercapacitor, Sliding Mode Controller, PI Controller, Fuzzy controller

I. INTRODUCTION

Smart cities utilize wireless sensor networks (WSNs) to manage their infrastructure and their resources efficiently. WSNs can monitor and control timely based information for society's comfort and safety, such as pollution detection, public surveillance, road traffic, smart grid monitoring, and many other applications [1]. However, one of the disadvantages of smart cities is to provide power to these devices since most of them are placed at remote locations. For example, the substructure cost for trenching and conduit installation to these devices is very high. Therefore, the need for energy harvesting is becoming vital as technology expands. An energy harvesting system allows for renewables sources to provide power to the load and, at the same time, to harvest energy.

Due to wireless sensor devices' remote placements, energy harvesting systems need to be reliable and sustainable to deliver power to these electrical devices. However, due to the unpredictable power generation of these renewables sources, such as photovoltaic (PV) and wind energy, energy storage is always necessary. An energy management system (EMS) is essential to continuously monitor the system by constantly sensing the system's voltage and current. Moreover, current and voltage controllers are needed to charge and discharge the energy storage.

Lithium-ion batteries are the primary energy storage device of power electronic devices because they have a high energy density, high efficiency, and a high life expectancy. However, they have a slower response compared to supercapacitors. On the other hand, a supercapacitor has a lower energy density than a battery, but it can respond to changes in power demand in hundreds of milliseconds, making them suitable for short-time demand [2]. The supercapacitors' advantages guarantee a longer lifetime in charge, charge speed, and instantaneous output power [3]. If only a lithium-ion battery is used as energy storage, the load suffers from a power drop due to the battery's slow time response.

Combining the battery and supercapacitor as energy storage accomplishes better power and energy performances on the system. The supercapacitor will cover the short-time energy demand of the load's fluctuation and the difference between the power demand and the battery response [4]. The battery covers the load's long-term energy demand when the renewable source does not provide enough energy to the load [5].

An energy management system for energy harvesting with lithium-ion battery and supercapacitor as energy storage is presented in this paper. The simulation results based on MATLAB/Simulink show that the supercapacitor covers shorttime load demand fluctuation. Therefore, the output power is kept constant compared to a system without a supercapacitor. The paper also conducts hardware and experimental analysis that establishes that the proposed system with a supercapacitor increases the time response of the power delivery to the load. The organization of the paper is as follows. The overall system section introduces the proposed system analyzed in this paper. The constant current (CC) and constant voltage (CV) controller section describe the SMC, Fuzzy, and PI controller for the charging algorithm. The simulation results show the obtained waveforms from the MATLAB/Simulink model for the proposed system. The experimental results present the realworld waveforms collected with the hardware presented in that section. Lastly, the conclusion summarizes the results.

II. OVERALL SYSTEM

The overall proposed system is shown in Fig. 1. As can be seen, the energy harvesting design has an energy management system that monitors the entire system. The system has a renewable source, photovoltaic source, as the primary energy source to the load, which mainly powers the low application device and charges the battery during daytime. It has a lithiumion battery and a supercapacitor as energy storage to power an electrical device when the renewable source does not produce enough energy.

Moreover, the presented block diagram shows that the lithium-ion battery and the supercapacitor are parallel to the DC-bus. This isolation configuration allows for current and voltage control of the battery and supercapacitor. In other words, the battery and supercapacitor power flow are actively controlled via the bidirectional DC-DC converters [4]. This introduces flexibility for the battery and supercapacitors voltage capacity since both are isolated from the dc-bus. However, this topology reduces the efficiency due to the losses in the DC-DC converters [4].

The EMS adjusts the battery and supercapacitor charge/discharge power to follow the load demand. The supercapacitor mainly covers short-time fluctuations, and the battery covers the long-time demand. The EMS monitors the battery since deep discharge and fast recharge can reduce the battery's life expectancy and capacity [6]. Therefore, during the charging state, when the renewable source produces enough energy to power the load and charge the battery, the EMS utilizes the CC and CV technique to charge the lithium-ion

battery. The current is controlled using the SMC controller, and the voltage is controlled using a typical PI controller.

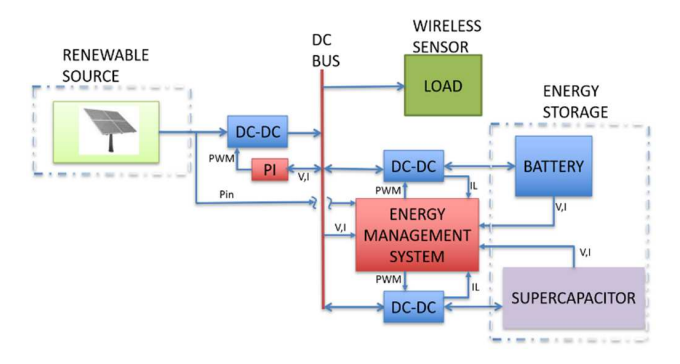


Fig. 1. Overall proposed system block diagram for energy harvesting with lithium-ion battery and supercapacitor

Typically, the voltage rating of a low power application device is 3 volts. Therefore, the system proposed targets 3.0V at dc-bus. Also, the power demand for the load is known since it is one of the EMS parameters to decide whether the battery and supercapacitor should be charged or discharged.

III. BIDIRECTIONAL DC-DC CONVERTER

The system uses a DC-DC buck converter to stabilize the renewable source input power and provide usable voltage. Also, it utilizes buck-boost DC-DC bidirectional converters to interface the DC-bus, where the load is connected, and the energy storage.

The buck converter steps down a higher input voltage to a lower output voltage. Operating the buck converter in the continuous conduction mode (CCM) can yield a steady-state input to output voltage transfer ratio of,

$$\frac{v_0}{v_i} = D \tag{1}$$

D is the duty ratio, Vo is the output voltage, and Vi is the input voltage [7]. Refer to the author [7] for other equations and detailed information.

The boost converter steps up a low input voltage to a higher output voltage. Operating the boost converter in the continuous conduction mode (CCM) yields a steady-state input to output voltage transfer ratio of,

$$\frac{\text{Vo}}{\text{Vi}} = \frac{1}{1-D} \tag{2}$$

D is the duty ratio, Vo is the output voltage, and Vi is the input voltage [7]. Refer to the author [7] for other equations and detailed information.

Fig. 2 shows a bidirectional buck-boost converter. The bidirectional converter is in buck mode when Q1 is on and Q2 is off [8]. On the other hand, the bidirectional converter is in boost mode when Q2 is on and Q1 is off.

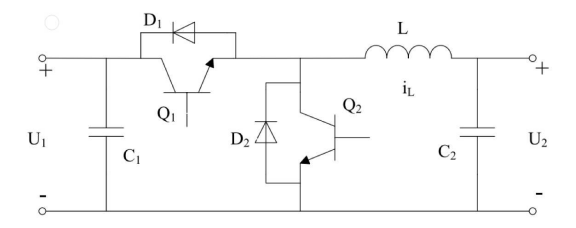


Fig. 2. Bidirectional buck-boost converter [8]

IV. ENERGY MANAGEMENT SYSTEM (EMS)

The EMS in this paper includes a battery management system to control and monitor the lithium-ion battery. Also, it consists of a supercapacitor management system to monitor and control the supercapacitor. As shown in Fig. 1, the energy management system controls the battery and supercapacitor's bidirectional converters based on the system current and voltage monitoring.

Fig. 3 shows the EMS control logarithm. As can be seen, the EMS allows charging of the energy storage if the Pin from the renewable source is greater than the load demand. However, if there is power fluctuation at the load, meaning that the desire power Pd < Pload, then energy storage discharges into the load. Note that due to its fast discharge, the supercapacitor discharges faster into the load.

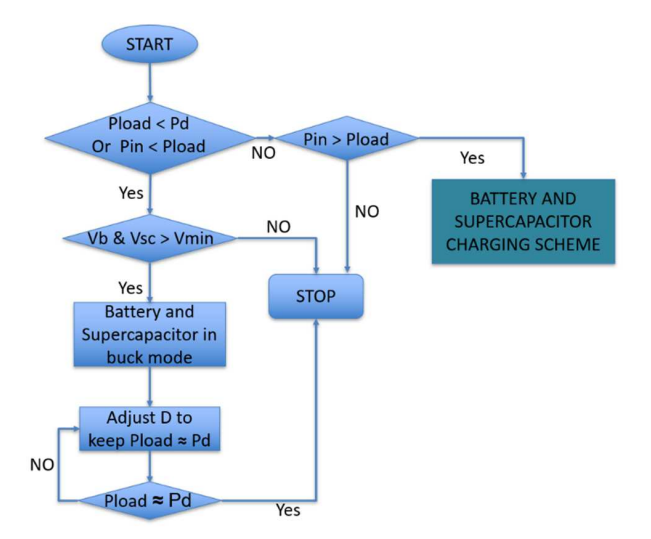


Fig. 3. EMS control algorithm

The DC-DC bidirectional converter's design depends on the system design input and output voltage based on the load.

A. Battery Management System

As shown in Fig. 4, the battery management system is the interface between the DC-bus and the lithium-ion battery. The battery management system improves battery efficiency and life expectancy by adjusting the charge and discharge rate through CV and CC using feedback controllers. As shown in Fig. 3, the bidirectional converter works in boost mode for this system when charging the battery. On the other hand, it works on buck mode when discharging the battery into the load.

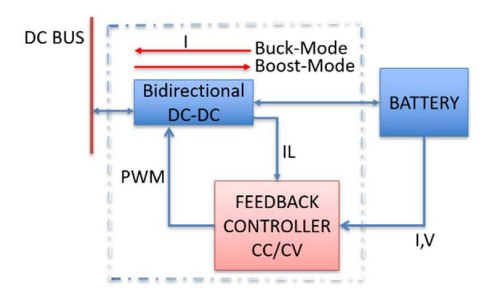


Fig. 4. Battery management system block diagram

Fig. 5 and Fig. 6 present the charging profile and the charging control algorithm for the lithium-ion battery. Note that the charging scheme is based on the CC and CV charging scheme. In this paper, 3.0 DC volts is targeted at the load's output to power a low power application wireless sensor network. Therefore, the lithium-ion battery's nominal voltage is 3.7V, and the maximum charging voltage is 4.2V. The battery current during the battery's constant charging state is 20% of the battery capacity. The cut-off battery current during the CV charging state shall be 1% of the battery capacity. During the battery discharge, the battery cut-off voltage shall be 80% of the nominal voltage. However, If the battery voltage drops below 3.0V, a preset CC of 10% of the battery capacity is applied to the battery until it reaches a preset voltage.

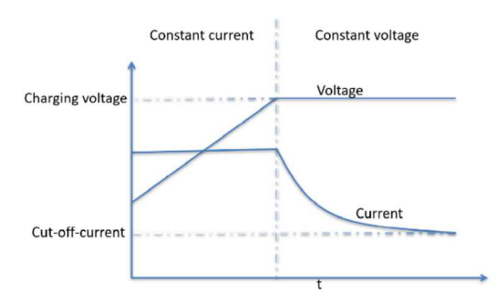


Fig. 5. Constant current and constant voltage charging profile for a single battery cell [9]

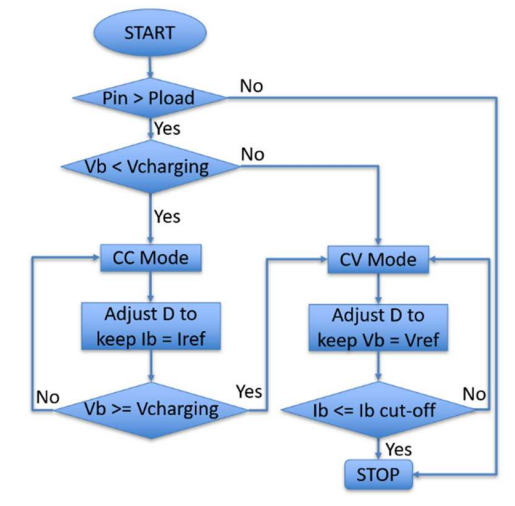


Fig. 6. Battery charging control algorithm [10]

Fig. 6 shows that the battery charging control algorithm does not charge the battery if the renewable source input power is less than the load demand. Also, based on the charging control algorithm, the voltage and current controllers will execute at different times depending on the battery's current and voltage state.

B. Supercapacitor Management System

The supercapacitor management system is the interface between the DC-bus and the supercapacitor. It is very similar to the battery management system. Therefore, the supercapacitor management system can be represented by the same block diagram of the battery management system in Fig. 4. The bidirectional converter works in boost mode when charging the supercapacitor and buck mode when the supercapacitor discharges into the load.

Fig. 7 and Fig. 8 presents the charging profile and the charging control algorithm for the supercapacitor. In this case, the charging scheme is based only on a CC. There is no need to charge the supercapacitor using a CV due to the supercapacitor's self-discharge. Therefore, the CC charges the supercapacitor until it reaches the desired voltage. Once the supercapacitor is self-discharged below this voltage, the current controller will execute once again.

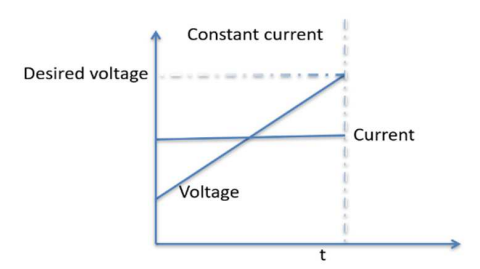


Fig. 7. Constant current charging profile for a supercapacitor

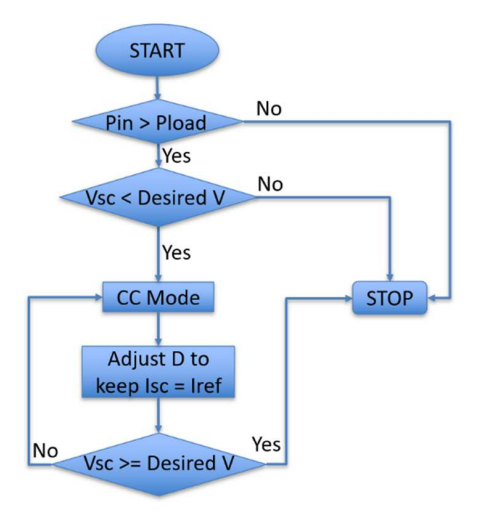


Fig. 8. Supercapacitor charging control algorithm.

Note that the supercapacitor charging is similar to the battery charging control algorithm. The supercapacitor charging control algorithm does not charge the supercapacitor if the renewable source input power is less than what the load needs.

V. CONSTANT CURRENT AND CONSTANT VOLTAGE CONTROLLER

The voltage and current controller's purpose is to maintain the current and voltage constant based on the charging profile and the charging control algorithm of the battery and supercapacitor. This is accomplished by adjusting the PWM duty cycle going into the gate of MOSFET of the DC-DC bidirectional converters.

A. Voltage Controller

A PI voltage controller provides a 3V constant from the renewable source to the DC bus. Also, it is present in the bidirectional converter when the battery discharges into the DC-bus during the buck-mode. Moreover, a 4.2V CV PI controller is used during the boost mode of the bidirectional dc-dc converter to charge the battery during the CV mode. Most of the time, to improve a PID controller's performance, the switching frequency could increase [11]. Therefore, the CV feedback control loop consists of a PI controller, providing zero state error.

$$Gc(s) = \frac{V_c(s)}{e(s)} = K_p + \frac{K_i}{s}$$
 (3)

$$Gc(s) = \frac{V_c(s)}{e(s)} = \frac{K_p s + K_i}{s}$$
 (4)

$$Gc(s) = \frac{V_c(s)}{e(s)} = K_p \frac{s + \frac{K_i}{K_p}}{s}$$
 (5)

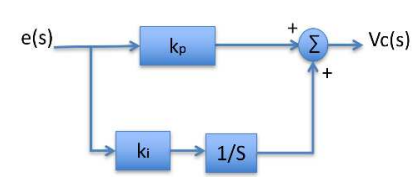


Fig. 9. PI voltage controller

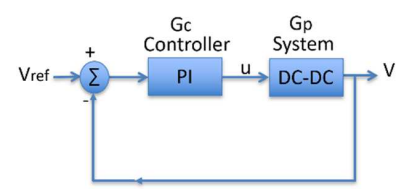


Fig. 10. System with PI controller

The following equation represents the close loop transfer function of Fig. 10, where Gc is the PI controller's transfer function, and the Gp is the DC-DC converter transfer function.

$$\frac{V(s)}{Vref(s)} = \frac{Gp(s)Gc(s)}{1+Gp(s)Gc(s)}$$
(6)

B. Current Controller

Fig. 11 represents the block diagram of the boost converter and a feedback sliding mode controller based on the following state equations of the boost converter.

$$\frac{\text{Di}_{L}}{\text{dt}} = -\frac{\text{V}_{o}}{\text{L}} + \frac{\text{V}_{o}}{\text{L}} u + \frac{\text{E}}{\text{L}} \tag{7}$$

$$\frac{dV_0}{dt} = \frac{i_L}{C} - \frac{i_L}{C} u - \frac{V_0}{RC}$$
 (8)

The i_L is the inductor current, E is the input voltage, Vo is the output voltage, L is the inductance, C and R are the capacitance and resistance. The variable u is the control input taking discrete values of 0 and 1 [12].

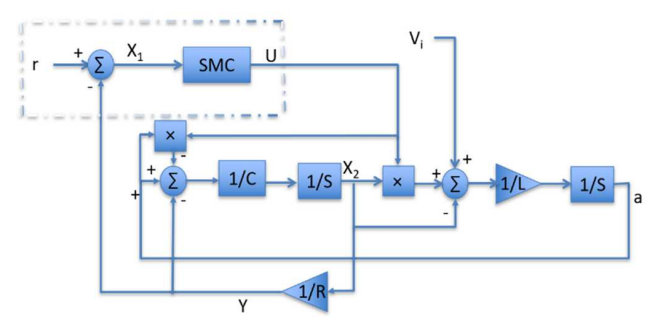


Fig. 11. Boost dc-dc converter block diagram with SMC current controller

To design the SMC, the error is X_1 , and Vo is designated as X_2 . Vi is the voltage at the DC bus. The control signal is $U=\varphi X_1$, and $\sigma = C_1 X_1 + X_2 = 0$ is the sliding line with slope C_1 . Y is the output current, and r is the current control signal reference.

$$X_1 = r - Y \tag{9}$$

$$\dot{X}_1 = -\dot{Y} \tag{10}$$

$$a = -\frac{1}{sL}(-X_2 + X_2U + Vin)$$
 (11)

$$\dot{X}_2 = \frac{1}{C} \left(-Ua + \frac{-X_2}{R} + a \right)$$
 (12)

$$\dot{X}_2 = \frac{1}{C} \left(\frac{-X_2}{R} + \frac{1}{sL} (-X_2 + X_2 \phi X_1 + Vin)(-X_1 \phi + 1) \right)$$
 (13)

$$\dot{\sigma} = C_1 \dot{X}_1 + \dot{X}_2 \tag{14}$$

$$\dot{X}_{2} = \frac{1}{C} \left(\frac{-X_{2}}{R} + \frac{1}{sL} (-X_{2} + X_{2} \phi X_{1} + Vin)(-X_{1} \phi + 1) \right) \gamma$$
 (15)

$$\dot{\sigma}\sigma = \frac{X_1}{C} \left[\frac{C_1}{R} + \frac{1}{sL} \left(\frac{Vin}{X_1} - C_1 \phi X_1 + C_1 \right) (-X_1 \phi + 1) \right] \gamma \sigma \quad (16)$$

$$\gamma = \left(-\frac{c_1}{R} + 1\right) \tag{17}$$

For the system to slide on σ , the designed controller must meet $\sigma\dot{\sigma}<0$.

For $X_1 \sigma < 0$,

$$\varphi < \left(\frac{Vin}{C_1 X_1} + 1\right) \frac{1}{X_1} \tag{18}$$

For $X_1 \sigma > 0$,

$$\varphi > \left(\frac{Vin}{C_1 X_1} + 1\right) \frac{1}{X_1}$$
 (19)

Therefore, by assuming a 2% error for the CC, Vin = 6V based on the PV panel, and choosing C_1 will get the φ gain for the sliding mode controller. Also, notice that as the gain increases to infinite, the error X_1 decreases to zero.

For comparison purposes, fuzzy logic and PI controllers are developed in this paper as CC controllers. Designing a closed-loop fuzzy logic controller for a DC-DC converter requires understanding the converter's behavior based on the desired output. The fuzzy logic controller block diagram is shown in Fig. 12. Note that the output signal from the fuzzy logic controller is the duty cycle, D.

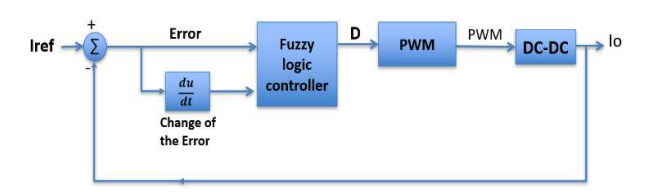


Fig. 12. Closed loop fuzzy logic CC for DC-DC converter

Fuzzy logic controller's fuzzification process creates crisp values from the two inputs using membership functions built based on linguistic values. Thus, the calculated crisp values are fed into the inference mechanism for decision making [13]. After that, the defuzzification converts the linguistic decisions into crisp control values using the Center of Gravity (COG) method (20) [14].

$$COG = \frac{\sum_{i=1}^{N} y_i \mu_{yi}}{\sum_{i=1}^{N} \mu_{yi}}$$
 (20)

Variable μ_{yi} is each fuzzy rule trigger degree, y_i is the output fuzzy set, and N is the number of rules. Hence, using COG with output membership function as shown in Fig. 13, the set of rules can be chosen as demonstrated in Table I. Moreover, smoothing the output is accomplished by reducing the rules that have a negative and positive large effect on the control output signal D.

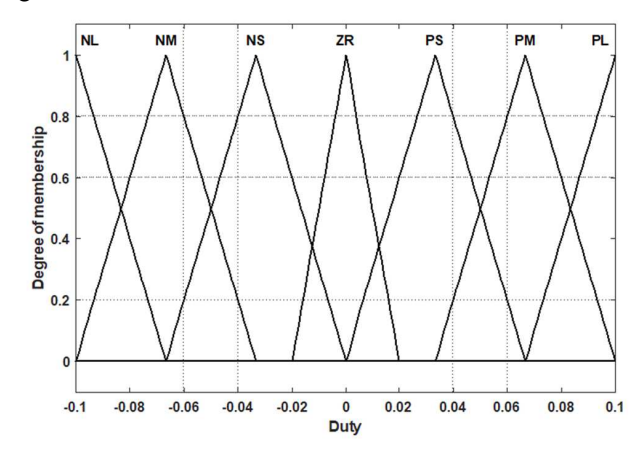


Fig. 13. Output membership functions

TABLE I. SETS OF RULES FOR FUZZY LOGIC CONTROLLER

Error Change of Error	NL	NM	NS	ZR	PS	PM	PL
NL	NL	NL	NL	NM	NM	NS	ZR
NM	NL	NL	NM	NM	NS	ZR	PS
NS	NL	NM	NM	NS	ZR	PS	PM
ZR	NM	NM	NS	ZR	PS	PM	PM
PS	NM	NS	ZR	PS	PM	PM	PL
PM	NS	ZR	PS	PM	PM	PL	PL
PL	ZR	PS	PM	PM	PL	PL	PL

The PI CC controller was implemented similarly to the PI CV controller shown in Fig. 9 and Fig. 10. The only difference is that the error is the sum of the desired current reference and the negative value of the actual current from the system. The K_p and K_i values for the CC controller were chosen based on (3) to (6).

VI. SYSTEM MODELING SIMULATION AND RESULTS

The overall system in Fig. 1 was model and simulated in MATLAB/Simulink. The model was simulated with time-varying irradiation, so that the power response at the load with and without supercapacitor was captured. The system task is to provide 60mW to the load. Fig. 14 shows the irradiation pattern utilized to observe the battery's charging and discharging into the load with and without the supercapacitor. Note that the renewable source between 0.7 and 1.1 seconds does not produce enough energy to power the load and charge the energy storage devices.

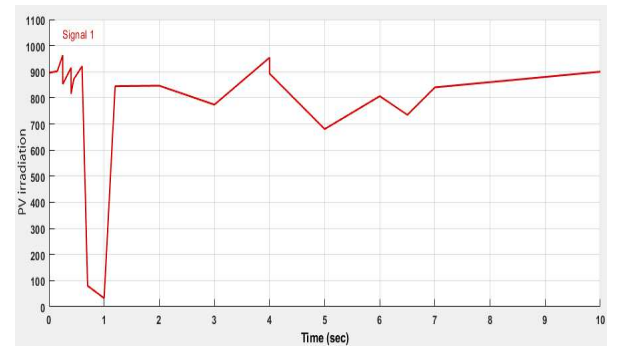


Fig. 14. PV input irradiation

Fig. 15 shows the power load's waveform based on the charging and discharging of the battery of the system without a supercapacitor. 100mA charging current was chosen to charge the battery to reduce power losses in the power converters. Note that there is a power drop between 0.7 and 1.1 seconds when Pin < Pload.

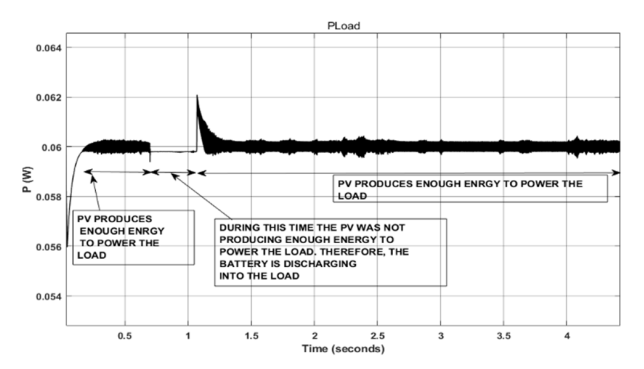


Fig. 15. Power load of the system without supercapacitor

On the other hand, Fig. 16 shows the power load's behavior based on the charging and discharging of the system's battery, which has a supercapacitor. However, to control the supercapacitor's power flow, a 40mA current controller was used to charge it. So, this will not cause high fluctuation on the dc-bus, where the load is connected. Notice that the waveform is much constant due to the fast discharge of the supercapacitor.

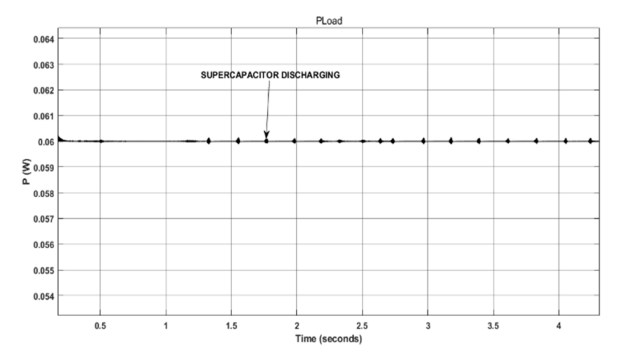


Fig. 16. Power load of the proposed system with supercapacitor

Based on Fig. 15 and Fig. 16, the system with supercapacitor outputs a more stable output power at the load, and it responds faster to a change in input power.

VII. EXPERIMENTAL IMPLEMENTATION AND RESULTS

The overall system shown in Fig. 1 was experimentally tested using real-world components. The photovoltaic panel is rated for 6W, Isc = 930mA, and Voc = 6V. The Lithium-ion battery is rated for a 1200mAh with a 3.7V nominal voltage, and 4.2V charging voltage. The bidirectional converter shown in Fig. 2 has capacitor C1 and C2 equal to 1000uF and the inductor L is 1mH, which reduces the ripples of the inductor current and improves the tracking reference current of the CC controller. The Supercapacitor used in the experimental and simulation is 470mF with a working voltage of 5V.

Fig. 17 shows the hardware implementation of the proposed energy harvesting system with a lithium-ion battery and a supercapacitor. As can be seen, the lithium-ion battery and the supercapacitor are connected to the designed PCB board for energy storage. The PCB designed has the bidirectional converters, the voltage, and the current sensor for the EMS system monitoring. Also, note that a DSP F28335 was utilized to interface the hardware to the EMS software implementation via MATLAB/Simulink.

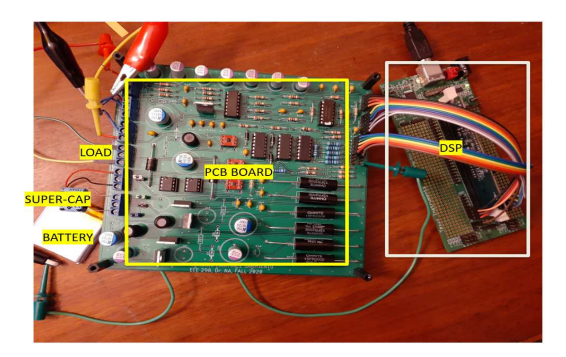


Fig. 17. Hardware implementation.

Fig. 18 and Fig. 19 show the battery current and the battery voltage based on the charging control algorithm. As can be seen, the battery first started charging at 100mA CC based on the reference current. Then, it was changed to 110mA to see if the SMC current controller could follow the reference charging current. Also, note that the current is noisy when the battery enters CV mode due to the controller trying to keep the voltage at 4.2V. However, the voltage oscillates at 4.2V, and this causes the system to oscillate between the current and voltage controller. Finally, the battery gets disconnected from the system once it reaches the cut-off current of 20mA, which indicates that it is fully charged based on the battery charging algorithm.

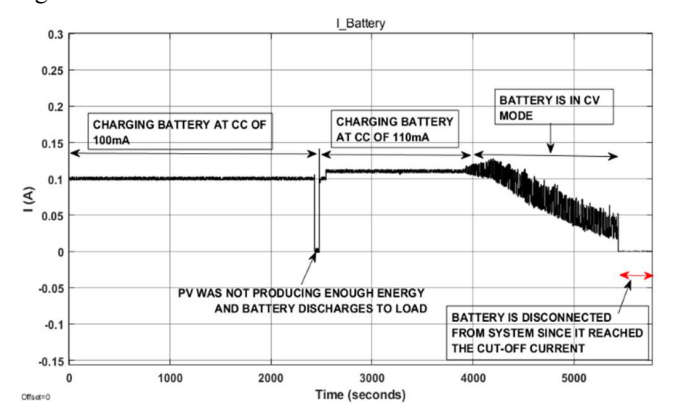


Fig. 18. Battery current (I_Battery)

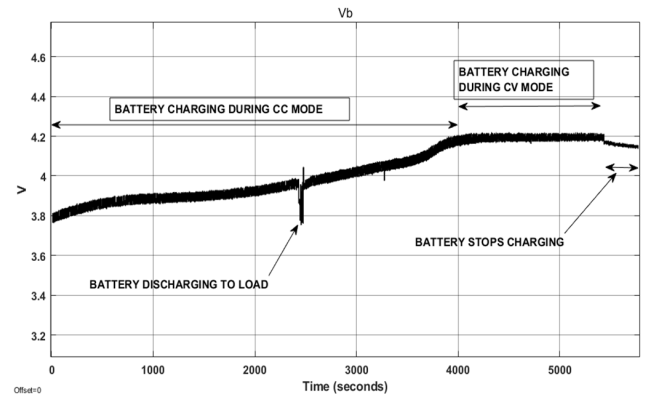


Fig. 19. Battery voltage (Vb)

Note that in Fig. 19, when the battery discharges into the load, the battery voltage jumps from 3.95V to 3.8V. Also, observe that after 4000s, the controllers charge the battery at a constant 4.2V as expected.

Fig. 20 shows the comparison between SMC, Fuzzy, and PI current controllers of the battery current. Table II compares the time response when the current reference value changes from 60mA to 100mA and from 100mA to 80mA. Note that during the 60mA to 100mA transition, the Fuzzy response is the fastest with a 760ms. On the other hand, during the transition from 100mA to 80mA, the SMC has the fastest response with 620ms. Also, based on Fig. 20, the SMC controller has the smallest current ripple. Therefore, it is used for charging in the EMS.

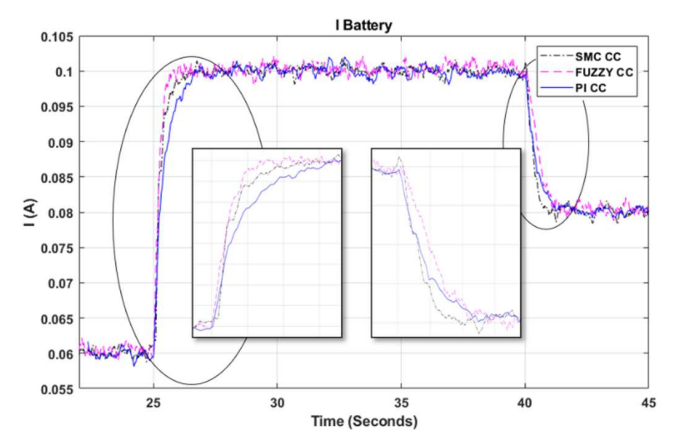


Fig. 20. SMC, Fuzzy, and PI CC controller for the battery current

TABLE II. SMC, FUZZY, AND PI CURRENT CONTROLLER TIME RESPONSES

CC Controller	Controllers			
CC Controller	PI	Fuzzy	SMC	
Time response of CC transition from 60mA to 100mA	1.65s	0.76s	1.43s	
Time response of CC transition from 100mA to 80mA	0.970s	0.840s	0.620s	

Fig. 21 shows the voltage load response of a system without a supercapacitor when the renewable source does not produce enough energy to power the load. In other words, the figure represents the voltage load response when the load experiences a transition of power source from PV to the battery. As can be seen, this transition caused a 1V voltage drop. Furthermore, it took around 207ms for the load voltage to recover to 3V.

Fig. 22 shows the system's voltage load response with supercapacitor when the renewable source does not produce enough energy to power the load. In other words, the figure represents the voltage load response when the load experiences a transition of power source from PV to the battery. As can be seen, this transition caused a 612mV drop. Furthermore, it took around 144ms for the load voltage to recover to 3V. Note that the response overshoots from 3V to 279mV due to the fast discharge of the supercapacitor. However, note that the controller recovered the output to the 3V reference faster than the system without the supercapacitor.

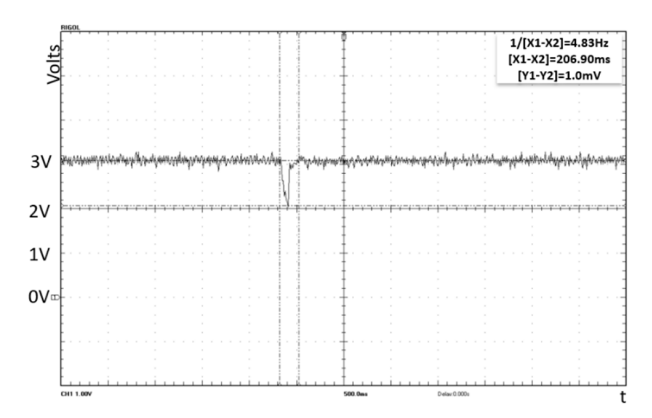


Fig. 21. Voltage load of the system without supercapacitor; Transition from PV to battery source

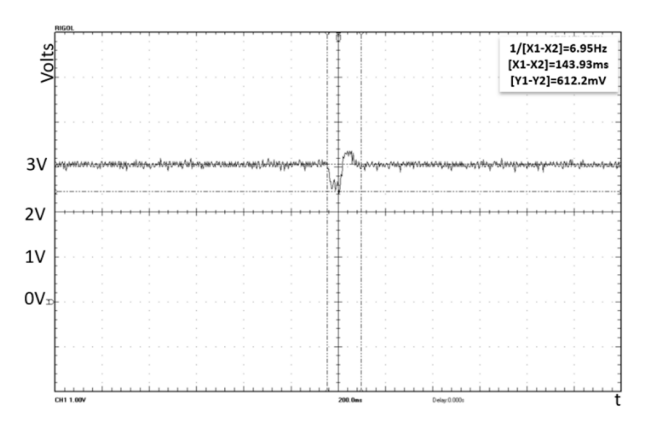


Fig. 22. Voltage load of the system with supercapacitor; Transition from PV to battery source

Table III shows the comparison results of a system with and without a supercapacitor, as demonstrated in Fig. 21 and Fig. 22. The table concludes that the proposed system with a supercapacitor responds 63ms, 30.4%, faster than a system that does not have a supercapacitor. However, the system with supercapacitor introduces an overshoot during the PV to battery power flow transition due to the rapid discharge of the battery and the PI controller's slow response.

TABLE III. VOLTAGE RESPONSE DUE TO A PV – TO – BATTERY TRANSITION

Energy	Data for PV to Battery Transition				
Harvesting System	Time response for transition PV - Battery	Voltage drop for transition PV - Battery	Voltage overshoot for transition PV -Battery		
System without supercapacitor	207ms	1V	none		
Proposed system with supercapacitor	144ms	612mV	279mV		

VIII. CONCLUSION

The overall goal was to design a sliding mode control-based energy harvesting system for low power applications. The system incorporates a supercapacitor to improve the response time of the system. The proposed design system with a supercapacitor was compared with a system without a supercapacitor. In the experimental data collected, the proposed method improved the response time of the system by 30.4%.

ACKNOWLEDGMENT

This paper is based upon work supported by the National Science Foundation Under Grant No. 1816197.

REFERENCES

- [1] R. Du, P. Santi, M. Xiao, A. V. Vasilakos and C. Fischione, "The sensable city: a survey on the deployment and management for smart city monitoring," in IEEE Communications Surveys & Tutorials, vol. 21, no. 2, pp. 1533-1560, Secondquarter 2019, doi: 10.1109/COMST.2018.2881008
- [2] Spataru, C., Kok, Y.C., Barrett, M.: 'Physical energy storage employed worldwide', Energy Procedia, 2014, 62, pp. 452–461
- [3] S. Saggini, F. Ongaro, C. Galperti and P. Mattavelli, "Supercapacitor-based hybrid storage systems for energy harvesting in wireless sensor networks," 2010 Twenty-Fifth Annual IEEE Applied Power Electronics Conference and Exposition (APEC), Palm Springs, CA, 2010, pp. 2281-2287, doi: 10.1109/APEC.2010.5433554.
- [4] W. Jing, C. Hung Lai, S. H. W. Wong and M. L. D. Wong, "Battery-supercapacitor hybrid energy storage system in standalone DC microgrids: areview," in *IET Renewable Power Generation*, vol. 11, no. 4, pp. 461-469, 15 3 2017.
- [5] Y. Zhang, Z. Jiang and X. Yu, "Control strategies for battery/supercapacitor hybrid energy storage systems," 2008 IEEE Energy 2030 Conference, Atlanta, GA, 2008, pp. 1-6, doi: 10.1109/ENERGY.2008.4781031.
- [6] N. K. Raghavendra and K. Padmavathi, "Solar charge controller for Lithium-Ion battery," 2018 IEEE International Conference on Power Electronics, Drives and Energy Systems (PEDES), Chennai, India, 2018, pp. 1-5.
- [7] Tasi-Fu Wu and Yu-Kai Chen, "Modeling PWM DC/DC converters out of basic converter units," in *IEEE Transactions on Power Electronics*, vol. 13, no. 5, pp. 870-881, Sept. 1998, doi: 10.1109/63.712294.
- [8] Chun Wang, Rui Xiong, Hongwen He, Xiaofeng Ding, Weixiang Shen, Efficiency analysis of a bidirectional DC/DC converter in a hybrid energy storage system for plug-in hybrid electric vehicles, Applied Energy, Volume 183, 2016, Pages 612-622, ISSN 0306-2619.
- [9] Leemput, Niels. (2015). Grid-supportive Charging Infrastructure for Plug-in Electric Vehicles.
- [10] Khan, Wajahat & Ahmad, Furkan & Alam, Mohammad. (2018). Fast EV charging station integration with grid ensuring optimal and quality power exchange. International Journal of Engineering Science. 1-10. 10.1016/j.jestch.2018.08.005.
- [11] L. Dinca and J. Corcau, "P.I. versus fuzzy control for a DC to DC boost converter," 2016 International Symposium on Power Electronics, Electrical Drives, Automation and Motion (SPEEDAM), Anacapri, 2016, pp. 803-808
- [12] H. Guldemir, "Sliding mode control of DC-DC boost converter," Journal of Applied Sciences, Vol. 5, No. 3, 2005, pp. 588-592.
- [13] K. Bendaoud et al., "Fuzzy logic controller (FLC): Application to control DC-DC buck converter," 2017 International Conference on Engineering & MIS (ICEMIS), 2017, pp. 1-5, doi: 10.1109/ICEMIS.2017.8272980.
- [14] E. Farshidi, "A low-power current-mode defuzzifier for fuzzy logic controllers," 2008 2nd International Conference on Signals, Circuits and Systems, 2008, pp. 1-4, doi: 10.1109/ICSCS.2008.4746941.